# Evaluation and comparison of JPSS VIIRS neural network retrievals of harmful algal blooms with other retrieval algorithms, validated against in-situ radiometric and sample measurements in the West Florida Shelf, and examination of impacts of atmospheric corrections, temporal variations and complex in-shore waters

Sam Ahmed[1], Ahmed El-Habashi[1], Vincent Lovko[2] and Michael Ondrusek[3]
[1]NOAA CREST Optical Remote Sensing Laboratory, the City College of New York, CUNY, New York, NY 10031, USA. Email: ahmed@ccny.cuny.edu, ahmed.elhabashi@gmail.com, [2]Mote Marine Laboratories, Sarasota, Florida, United States Email: vlovko@mote.org, [3]NOAA /NESDIS 5830 University Research Court, College Park, MD 20740 Email: Michael.Ondrusek@noaa.gov.

## ABSTRACT

We examine the potential for ocean color (OC) retrievals using a neural network (NN) technique recently developed by us to make up for the lack of a 678 nm florescence band on VIIRS, previously available on MODIS and important for *Karenia brevis* harmful algal bloom (*KB* HABs) retrievals.. NN uses VIIRS Remote Sensing Reflectance (Rrs) at 486, 551 and 671 nm to retrieve phytoplankton absorption at 443nm, from which both *KB* HABs and chlorophyll [*Chla*] concentrations can be inferred. NN retrievals are compared with retrievals obtained using other algorithms, including OCI/OCx and Semi-analytical algorithm for both complex and open ocean waters. VIIRS *KB* HABs retrievals in the WFS, using NN and other algorithms, are first compared against all co-incident in-situ cell count measurements available between 2012-16. Next, we compared retrievals obtained for different algorithms using in-situ radiometric Rrs measurements against sample measurements, 2017-18, for both the WFS and Atlantic coasts. Retrieval statistics showed (i) the important impact of short term (15-20 minutes) temporal variations and sample depth considerations in complex bloom waters. These limit satellite retrieval accuracies and utility; and (ii) particularly for high chlorophyll bloom waters, better retrieval accuracies were obtained with NN followed by OCI/OCx algorithms. Likely rationales: the longer Rrs wavelengths used with NN are less vulnerable (i) to atmospheric correction inadequacies than the deeper blue wavelengths used with other algorithms, and (ii) to spectral interference by CDOM in more complex waters.

**Keywords:** neural networks; harmful algal blooms; ocean color remote sensing reflectance; *Karenia brevis*; retrieved chlorophyll-*a*; normalized fluorescence height; West Florida Shelf**.**

## 1. INTRODUCTION

We have previously described a NN approach [1, 2] for the detection and tracking of *KB* HABs that frequently plague the coasts and beaches of the West Florida Shelf (WFS) using VIIRS satellite data. Effective *KB* HABs detection and tracking approaches are needed for use with the VIIRS satellite. These are needed so that NOAA can extend to VIIRS, its *KB* HABs monitoring capabilities, which previously relied on MODIS-A imagery [3-9] and specifically on (*Rrs*678) the remote sensing reflectance signal at 678nm, the chlorophyll fluorescence wavelength. (*Rrs*678) was used with MODIS-A in the normalized fluorescence height [2-4] and related Red Band Difference (RBD) [3] techniques to help in *KB* HABs retrievals. However, the current VIIRS satellite, unlike its predecessor MODIS-A, does not have a 678 nm channel to detect chlorophyll fluorescence. To overcome the lack of a fluorescence channel on VIIRS, the NN approach bypasses the need for measurements of chlorophyll fluorescence, allowing us to extend *KB* HABs satellite monitoring capabilities in the WFS to VIIRS.

In the previous work [1, 2], results showed the efficacy of a NN approach for detecting *Karenia* brevis (*KB*) harmful algal blooms (HABs) in the West Florida Shelf (WFS). The essence of the approach is the application of a standard multiband neural network (NN) inversion algorithm, previously developed and reported by us [1, 10-13]. This takes VIIRS *Rrs* measurements at the 486, 551 and 671 nm bands (or 488, 555, and 667 nm bands for MODIS-A) as inputs. It then produces related inherent optical properties (IOPs) at 443 nm as its outputs, among them, the absorption coefficients

Remote Sensing of the Ocean, Sea Ice, Coastal Waters, and Large Water Regions 2018,
edited by Charles R. Bostater, Stelios P. Mertikas, Xavier Neyt, Proc. of SPIE Vol. 10784,
1078402 · © 2018 SPIE · CCC code: 0277-786X/18/$18 · doi: 10.1117/12.2325749

of phytoplankton, ($a_{ph443}$). The NN is used to generate an $a_{ph443}$ image of the WFS, which is then converted into an equivalent [*Chla*] image, using empirical relationships for specific chlorophyll absorption values in the WFS, which have been determined from *in situ* measurements [14]. Then, to obtain *KB* HABs values from the VIIRS NN retrieved $a_{ph443}$ image, we apply to it two filter processes. These filters are based on constraints known to be associated with *KB* HABS in the WFS. These are: (i) low backscatter at 551 nm, manifested as a maximum permissible value of $Rrs551 \leq Rrs551\text{max}$ and (ii) a minimum permissible [*Chla*]min threshold value [9, 15] and hence an equivalent minimum permissible value: $a_{ph443} \leq a_{ph443\text{min}}$. Following application of these two filter processes, the residual image will only show $a_{ph443}$ values that are compatible with both criteria for *KB* HABs, and are therefore representative of *KB* HABs. VIIRS retrievals of *KB* HABs in the WFS, using our NN technique, were compared with those obtained using other retrieval algorithms, and all retrievals were also evaluated against data sets of in-situ measurements. These comparisons showed the NN technique to be generally the most effective in terms of retrieval accuracies [2].

In this work, OC retrievals using NN are compared with retrievals using other algorithms, including OCI/OCx and Semi-analytical algorithm for both complex and open ocean waters. First, VIIRS *KB* HABs retrievals in the WFS, using NN and other algorithms (including OCI/OCx, GIOP, QAA and RGCI), are compared against all co-incident in-situ cell count measurements available over the 2012-16 period. These data sets cover the available data from the start of the VIIRS mission in January 2012 to 2016. In these comparisons, the NN technique was again found to exhibit the best retrieval accuracy statistics. The results also highlighted the impact of temporal variations on achievable retrieval accuracies.

Next, we obtained retrievals for NN and the other algorithms using in-situ radiometric Rrs measurements as inputs, and compared these retrievals against in-situ sample measurements, for both the WFS and Atlantic coasts. Here, the use of in-situ Rrs measurements eliminates the impact of possibly inadequate atmospheric correction procedures that can affect satellite Rrs retrievals. Retrieval statistics confirmed (i) the important impact of short term (15-20 minutes) temporal variations and sample depth considerations in complex bloom waters. These limit satellite retrieval accuracies and utility; and (ii) particularly for high chlorophyll bloom waters, better retrieval accuracies were obtained with NN followed by OCI/OCx algorithms. Likely rationales are that: the longer Rrs wavelengths used with NN are less vulnerable (i) to atmospheric correction inadequacies than the deeper blue wavelengths used with other algorithms, and (ii) to spectral interference by CDOM, expected in more complex coastal waters. Examination of sequential satellite observations of the WFS also show the importance of short term temporal variabilities and underline their impact on accuracies of retrievals. Finally, field measurements of Sarasota, FL confirm the temporal variability of *KB* HABs and their patchiness in the WFS.

## 2. MATERIALS AND METHODS- BACKGROUND

### 2.1 Neural network algorithm background

For development of our NN algorithm [1, 10-13] a synthetic data set of 20,000 IOPs, was produced based on the NASA Bio-Optical Marine Algorithm Data set, (NOMAD) [16]. These IOPs, whose range and variability is well represented in the literature [17-21] were then used as inputs to a four component bio-optical model [12, 20, 21] which in conjunction with a HydroLight based [22], parameterized forward model, described in Lee 2002 [20] produced 20,000 sets of *Rrs* values at 486, 551 and 671 nm (for VIIRS) and at 488, 555 and 667 nm for MODIS. The NN was trained on 10,000 of these values and tested on the 10,000 remaining subset, as well as on field data to solve the inverse problem [23] of retrieving physical variables, including $a_{ph443}$, from *Rrs* values at 486, 551 and 671 nm, and at 488, 555 and 667 nm. The algorithm is a standard multiband NN inversion algorithm that takes VIIRS *Rrs* measurements at the 486, 551 and 671 nm bands and MODIS measurements at 488, 555 and 667 nm bands, in the WFS as inputs, and produces as outputs the related IOPs, namely: $a_{ph443}$, $a_g$ and $a_{dm}$ as well as $bb_p$, all at 443 nm. (As mentioned in the introduction, it is only with the $a_{ph443}$ output of NN that we are concerned with here). Detailed descriptions of the NN are given in Refs. [10-13], and [1] gives the necessary parameters for implementation of the NN with a MATLAB tool for obtaining satellite retrievals.

## 3. RESULTS: EVALUATION OF VIIRS *KB* HABS RETRIEVALS, OBTAINED USING NN AND OTHER ALGORITHMS, AGAINST AVAILABLE IN SITU MEASUREMENTS

### 3.1 Algorithms considered for VIIRS retrievals of *KB* HABs.

In the following sections, we focus on comparing VIIRS [*Chla*] and retrievals against coincident or near coincident in-situ measurements of *KB* cell counts and their equivalent [*Chla*]. In this work we expand comparisons of retrievals using NN to retrievals using OCI/OCx [24], RGCI [25], and the widely used GIOP [26-28] and QAA [20, 29, 30] algorithms. The salient features of these different retrieval algorithms are summarized below.

The OCI and OCx indexes [31, 32], are the default NASA products [24] that retrieve the near surface chlorophyll-a concentrations [*Chla*]. The product uses a combination of the OCx and OCI algorithms. The OCx algorithm is adapted to retrieve [*Chla*] in eutrophic waters ($\geq 0.4\ \mu g\ L^{-1}$) where OCI algorithm is adapted to retrieve [*Chla*] in oligotrophic oceans ($\leq 0.25\ \mu g\ L^{-1}$). The transition between the two algorithms occurs through blending of the OCI/OCx algorithm. OCx is a fourth-order polynomial empirical relationship that makes use of the blue/green Rrs ratio. OCI is based on a three-band reflectance difference that estimates Chlorophyll-a concentrations from the relative height of the green band and a baseline formed linearly between the blue and red bands.

GIOP - Generalized Inherent Optical Property (GIOP) model. While there are numerous Semi-analytical algorithms (SAAs) exist to estimate IOPs, GIOP allows construction, evaluation and selection of specific modeling assumptions from different SAAs at runtime, in order to generate a unified IOP model. This NASA algorithm [26-28] returns spectral marine absorption and backscattering coefficients for water column constituents (e.g., colored dissolved organic material (CDOM) and algal and non-algal particles) in $m^{-1}$, calculated using the default global configuration of the Generalized Inherent Optical Property (GIOP) model. We use it here to retrieve [*Chla*] from VIIRS observations for match-ups with in-situ measurements.

QAA - Quasi-Analytical Algorithm version 5 (QAA_5) [20, 29, 30], developed by *Lee et al.* [2002] to derive the absorption and backscattering coefficients by analytically inverting the spectral remote-sensing reflectance ($Rrs(\lambda)$). It starts with an empirical estimate of the total absorption coefficient at a reference wavelength (550, 555 or 560) and then analytically calculates the backscattering coefficient at the same wavelength. The amplitude of these coefficients at other wavelengths is obtained using an empirical estimate of the particulate backscattering spectral shape and the measured remote-sensing reflectance. After the total absorption coefficient is known, it can be further decomposed into the algal and non-algal components. We use it here to retrieve [*Chla*] from VIIRS observations for match-ups with in-situ measurements.

RGCI-Red Green Chlorophyll Index. RGCI is an empirical WFS region specific retrieval algorithm [25] that retrieves [*Chla*] from observations of MODIS-A and VIIRS bands. For VIIRS, the [*Chla*] retrievals are given by:

$$[Chla]_{RGCI} = 0.1 \times \exp\left(11.8 \times \frac{Rrs671}{Rrs551}\right)\ , \mu g\ L^{-1} \qquad (1)$$

The above algorithms, all-applicable with VIIRS, will be those used in retrieval comparisons against in-situ measurements and comparisons against VIIRS NN.

### 3.2 In-situ measurement data sets for comparisons of VIIRS retrievals of *KB* HABs.

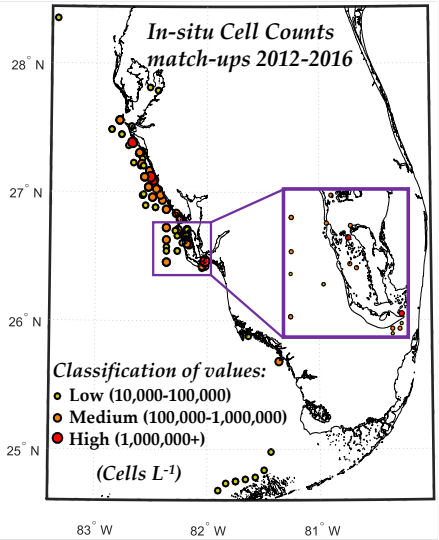


Figure 1 showing in-situ locations of *Karenia* brevis cell counts covering the range 0.01–9.2x$10^6$ cells·L−1 and collected by the Florida Fish and Wildlife Conservation Commission (FWC). Zoomed areas illustrate the extent of the underlying details of *KB* values available in VIIRS retrievals for the period of 2012–2016.

The ultimate test for the viability of *KB* HABs satellite retrieval techniques is their ability to match retrieved values with concurrent *in situ* measurements. However, it is difficult on any one day to find sufficient matchups between satellite observations and concurrent, or near concurrent *in situ* measurements to obtain statistically meaningful results. We therefore extended the study period to look at all available WFS match-ups, Fig. 1, between VIIRS measurements and *in situ* data at concurrent dates and over the 2012–2016 period for which there was available VIIRS data.

We then looked for match ups where the overlap time windows between satellite observations and in-situ measurements were 15 minutes and 100 minutes. The 100 minutes time window conforms to the approximate time between consecutive VIIRS overpasses, and therefore of consecutively retrieved images. These can therefore provide evidence of the temporal variations, observed with *KB* HAB blooms. The shorter 15-minute time window was selected after an investigation that found 15 minutes to be the shortest time window, which at the same time provided enough match up data points for meaningful statistical analysis. This approach is borne out by the results which show much better match ups for the 15 minutes window. This has important implications regarding the validity of satellite observations of *KB* HABs.

### 3.3 Comparisons of VIIRS retrievals using NN and other algorithms against *KB* HABs in-situ measurements in the WFS over the 2012-16 period for 100 minutes and 15 minutes windows between the overpass time and in-situ observations.

When comparisons were being made between retrievals using NN and OCI/OCx and RGCI algorithms, it was found that there were 23 match-ups of available in-situ measurements that satisfy the match-up conditions for satellite observations within a 15 minutes overlap time window. The additional conditions stipulated for match-up were that pixel centers were 0.3 miles or less from the in situ measurement location. This is an empirical approach to ensure that pixel values could be reasonably assumed to reflect the related in-situ measurements and hence reduce potential impact of patchiness [33] within the pixel (0.7 $Km^2$ and 1.0 $Km^2$ corresponds to nadir observation for VIIRS and MODIS respectively). Pixels were also excluded from the match-up comparisons if they had been flagged for any of the following: land, clouds, failure in atmospheric correction, stray light, bad navigation quality, both high and moderate glint, negative Rayleigh corrected radiance, viewing angle greater than 60°, and solar zenith larger than 70°, as well as any pixels which had water leaving radiance spectra with negative values in any one wavelengths. Cell counts sample measurements also had to be at less than 1 meter depth, and at concentrations $\geq 10^4$ cells·$L^{-1}$. It should be noted that [*Chla*] of 1 µg·$L^{-1}$ is taken as ~$10^5$ cells·$L^{-1}$ [34]. The in situ cell count data was obtained from the Florida Fish and Wildlife Conservation Commission's Fish and Wildlife Research Institute (FWC-FWRI). The search for match-up between VIIRS satellite and in-situ observations on the same day and within a 100 minute window of the overpass time

showed 93 cases which satisfied the match-up conditions as specified above. The seasonal distribution of these 93 match-ups between satellite observations and in-situ measurements used in the comparison of retrieval accuracies is shown in Table 1 below.

**Table 1.** Seasonal distribution of match-ups used in the comparison of retrieval accuracies.

| *January 2012-March 2016* | *Winter* | *Spring* | *Summer* | *Fall* | *Total* |
|---|---|---|---|---|---|
| ***Number of match-ups*** | 18 | 6 | 1 | 68 | 93 |

Fig. 2 shows the relationship between retrieved [*Chla*] using the NN, OCI/OCx and RGCI algorithms and the in-situ *KB* cell count measurements for the 100 minute and 15 minute match up time windows are shown. For NN, OCI/OCx and RGCI retrievals it was found there were 93 valid observations within the 100-minute window between overpass time and the in-situ measurements. The matchup results for the 100 minute window are shown in the upper row. In these results, $R^2$ is the coefficient of determination. To determine $R^2$ the orthogonal linear regression approach (OR) was used where errors are assumed to exist for both variables. The error (ε) is calculated as the sum of orthogonal distances. OR estimates of $X$ on $Y$ will minimize the orthogonal distance from the observed data points to the regression line [35].

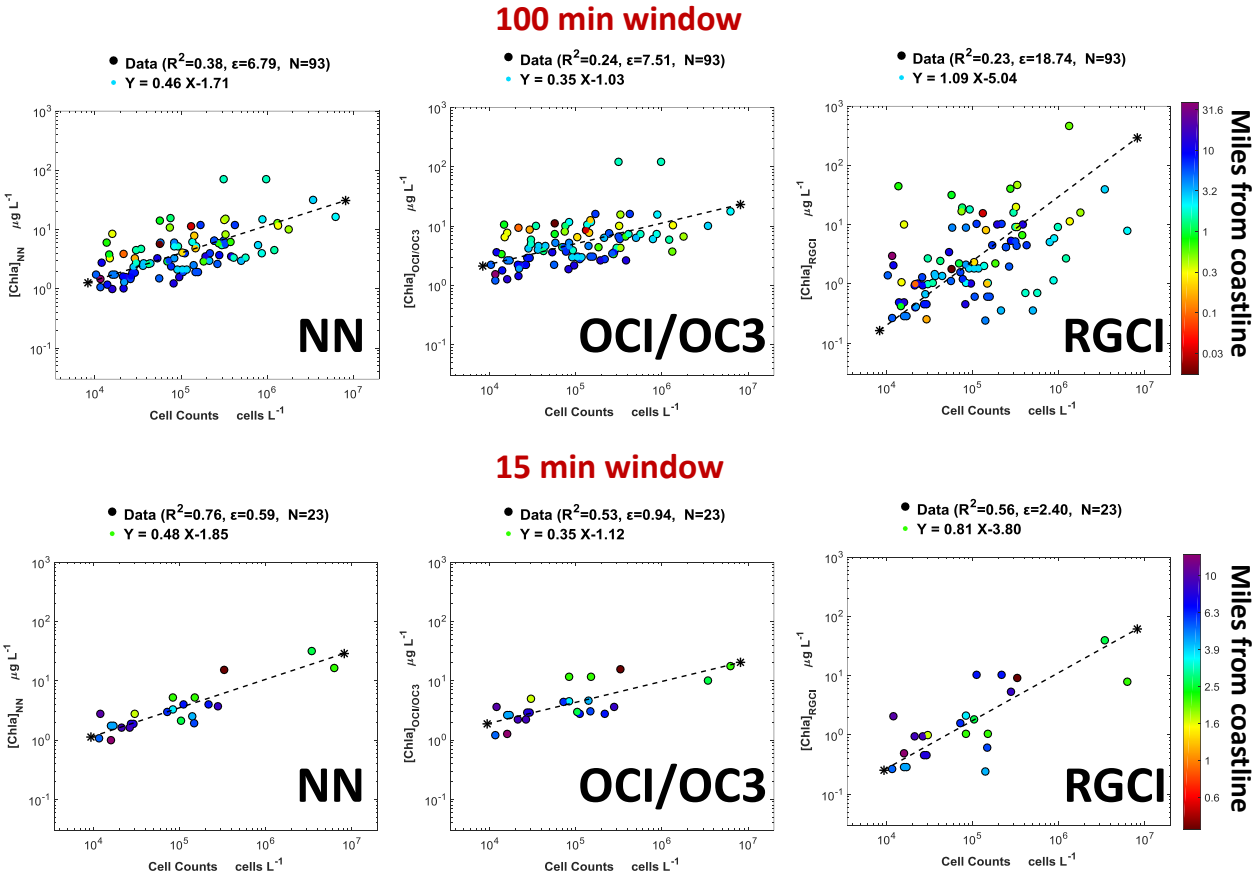


Figure 2 showing in-situ comparison for the available match-ups points for 100 and 15 minutes overlap windows with in-situ observations obtained using the different algorithms (NN, OCI/OCx, and RGCI). Color-coding of the dots denotes distance to shore, with red being the closest.

Fig. 2 (row) shows the results for the 23 match-ups obtained when the observations window between overpass time and in-situ measurements is restricted to 15 minutes, during which the impact of temporal variations is reduced. As can be seen, correlations and errors greatly improve for the 15-minute window, compared to the 100-minute window

observations. It is also observed that NN retrievals exhibit the best performance for both time windows, in terms of both correlations and errors.

When VIIRS retrievals comparisons were extended to retrievals using GIOP and QAA algorithms, it was found that both algorithms exhibited negative values or no retrievals in many instances. When these negative values are excluded, there remained 68 valid match-ups for the 100-minute overpass window. The retrieved [*Chla*] for these 68 match-ups is shown against in-situ cell counts in Fig. 3, for all retrieval techniques.

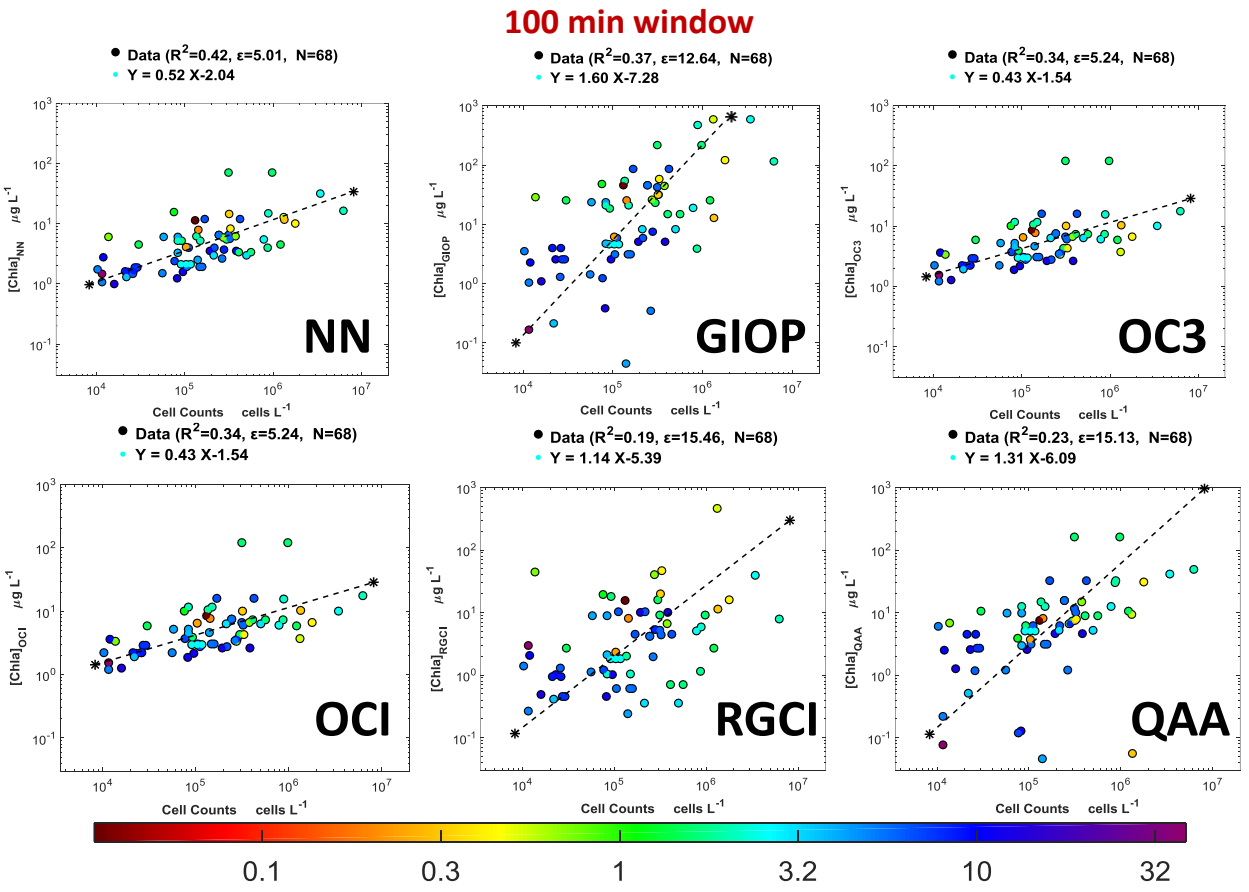


Figure 3 Results for 68 in-situ observations within 100 minutes of VIIRS overpass for the six algorithms showing retrieved [*Chla*] against *KB* HABs cell counts for NN, GIOP, OC3, OCI, RGCI, and QAA retrievals; Color coding of the dots denotes distance to shore, with red being the closest (miles from coastline).

When the overlap observation window is reduced to 15 minutes, we have 18 valid match-ups remaining, after excluding negative values associated with GIOP and QAA. Results for these 18 match-ups are shown in Fig. 4 below. Again, as can be seen, correlations and errors greatly improve for the 15-minute window over those for the 100-minute window, Fig. 3.

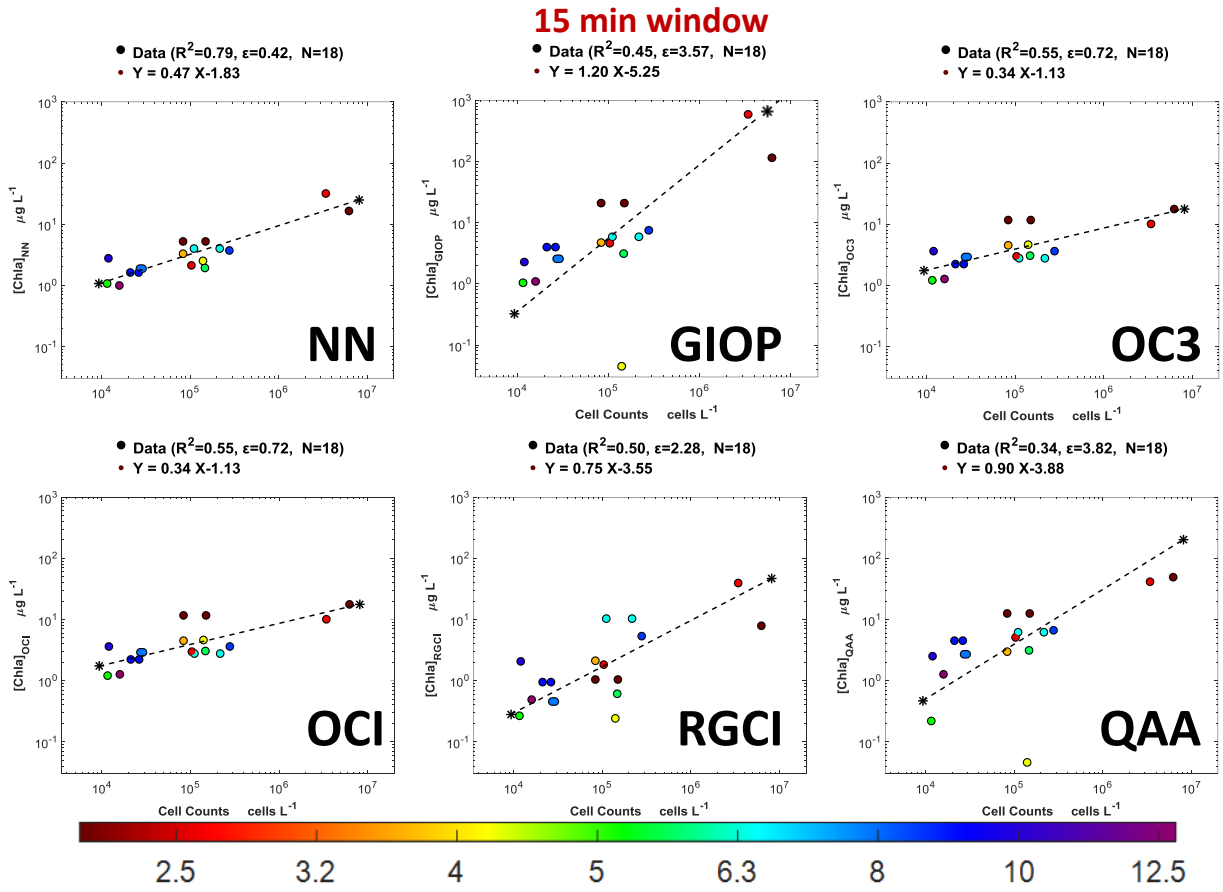


Figure 4 Results for 18 in-situ observations within 15 minutes of VIIRS overpass for the six algorithms showing retrieved [*Chla*] against *KB* HABs cell counts for NN, GIOP, OC3, OCI, RGCI, and QAA retrievals ; Color coding of the dots denotes distance to shore, with red being the closest (miles from coastline).

The results in Figs. 3 and 4, which illustrate the impact of observation time windows on retrieval accuracies for all algorithms are summarized in Tables 2 and 3 below. These results support the conclusion, that, at least for these preliminary and somewhat limited data sets, the NN retrievals exhibit the best performances against the in-situ measurements, for both the longer (100-minute) and, more importantly, the shorter (15-minute) overlap time windows. This was observed both in terms of higher correlations and in terms of lower errors against the in-situ measurements.

**Table 2** Comparison statistics for Fig. 2:

| ***y-axis*** ***[Chla]*** *(µg·L$^{-1}$)* | ***x-axis*** ***KB*** *Cell Counts (cells L$^{-1}$)* | $R^2$ | $\varepsilon$ | ***Slope & Intercept*** | ***N*** |
|---|---|---|---|---|---|
| ***NN*** | VIIRS 100 minutes window | 0.38 | 6.79 | $y = 0.46\,x - 1.71$ | 93 |
| ***OC3*** | | 0.24 | 7.51 | $y = 0.35\,x - 1.03$ | 93 |
| ***OCI*** | | 0.24 | 7.51 | $y = 0.35\,x - 1.03$ | 93 |
| ***RGCI*** | | 0.23 | 18.74 | $y = 1.09\,x - 5.04$ | 93 |
| ***NN*** | VIIRS 15 minutes window | 0.76 | 0.59 | $y = 0.48\,x - 1.85$ | 23 |
| ***OC3*** | | 0.53 | 0.94 | $y = 0.35\,x - 1.12$ | 23 |
| ***OCI*** | | 0.53 | 0.94 | $y = 0.35\,x - 1.12$ | 23 |
| ***RGCI*** | | 0.56 | 2.40 | $y = 0.81\,x - 3.80$ | 23 |

**Table 3** Statistics of comparison for Figs. 3 and 4:

| *y-axis* *[Chla]* ($\mu g \cdot L^{-1}$) | *x-axis* *KB Cell Counts* (cells $L^{-1}$) | $R^2$ | $\varepsilon$ | *Slope & Intercept* | *N* |
|---|---|---|---|---|---|
| ***NN*** | VIIRS 100 minutes window | 0.42 | 5.01 | $y = 0.52x - 2.04$ | 68 |
| ***GIOP*** | | 0.37 | 12.64 | $y = 1.60x - 7.28$ | 68 |
| ***OC3*** | | 0.34 | 5.24 | $y = 0.43x - 1.54$ | 68 |
| ***OCI*** | | 0.34 | 5.24 | $y = 0.43x - 1.54$ | 68 |
| ***RGCI*** | | 0.19 | 15.46 | $y = 1.14x - 5.39$ | 68 |
| ***QAA*** | | 0.23 | 15.13 | $y = 1.31x - 6.09$ | 68 |
| ***NN*** | VIIRS 15 minutes window | 0.79 | 0.42 | $y = 0.47x - 1.83$ | 18 |
| ***GIOP*** | | 0.45 | 3.57 | $y = 1.20x - 5.25$ | 18 |
| ***OC3*** | | 0.55 | 0.72 | $y = 0.34x - 1.13$ | 18 |
| ***OCI*** | | 0.55 | 0.72 | $y = 0.34x - 1.13$ | 18 |
| ***RGCI*** | | 0.50 | 2.28 | $y = 0.75x - 3.55$ | 18 |
| ***QAA*** | | 0.34 | 3.82 | $y = 0.90x - 3.88$ | 18 |

Retrieval accuracies for the 15 minute window for NN, OCI/OCx and RGCI as a function of distance from shore are shown in Fig. 5 below, where NN shows better accuracies, followed closely by OCI/OCx

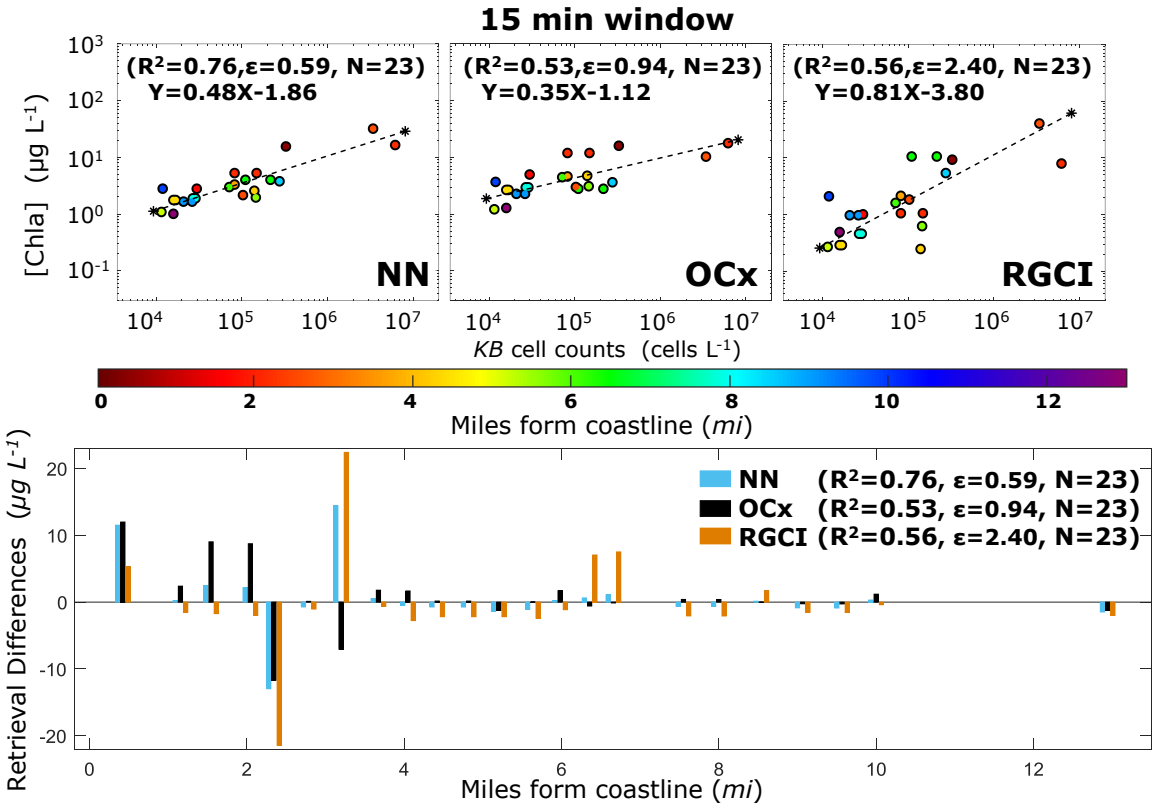


Fig. 5 Retrieval accuracies as a function of distance from land for the 15 minute overpass window for NN, OCI/OCx and RGCI.

### 3.4 The use of Consecutive satellite images to examine temporal changes

From the results in 3.3 above, it was seen that reducing the time window between satellite and in situ observations can generally significantly increase the accuracy between VIIRS retrieved [*Chla*] and in-situ measured *KB* cell counts. These changes can be quite rapid [36]. To explore the potential for detecting HAB bloom changes over relatively short periods from overlapping consecutive satellite overpasses, we have also examined changes in three consecutive overlapping satellite images in Figs. 6. Two of these are from VIIRS, 96 minutes apart and an intermediate one is from MODIS-A, 70 minutes after the first VIIRS image.

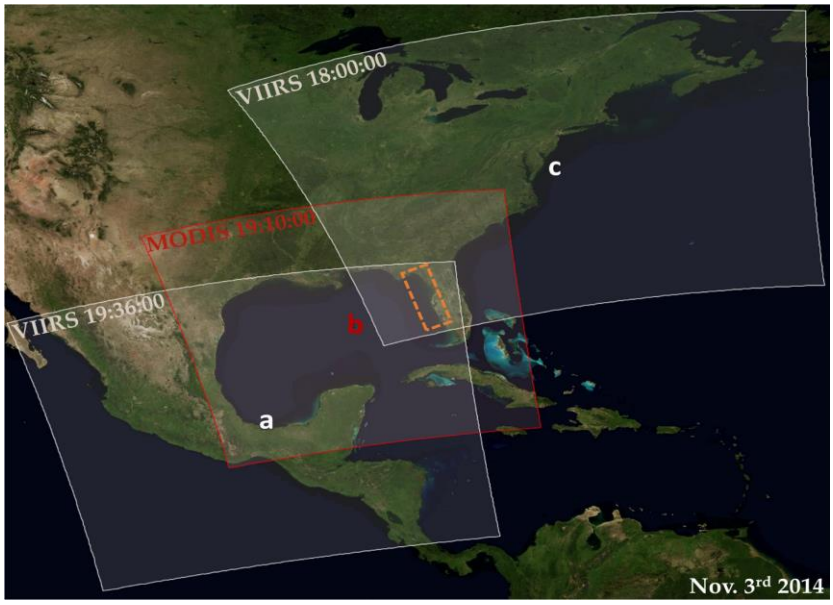


Figure 6 the MODIS-A granule and two VIIRS Granule within 100 minutes on Nov. 3rd 2014.

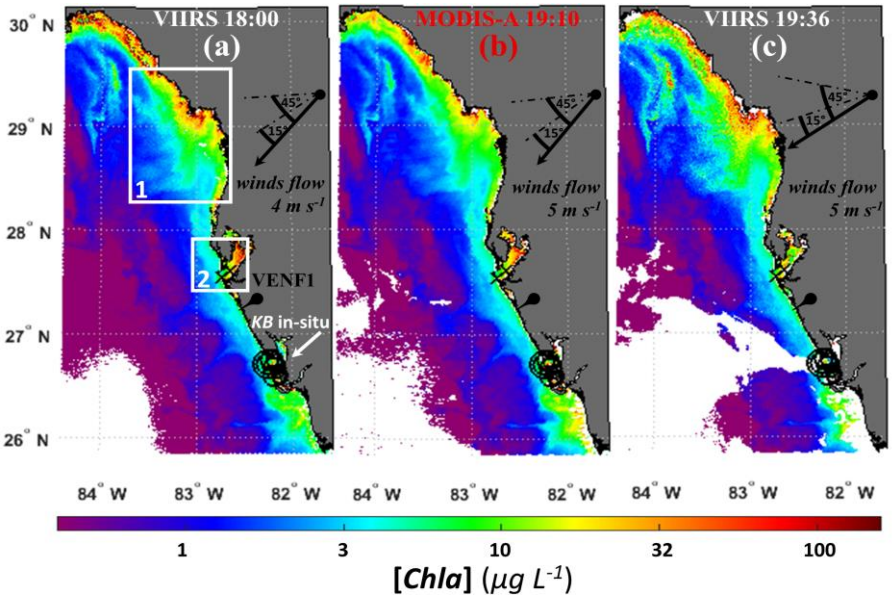


Figure 7 a, b and c showing temporal changes in bloom for consecutive satellite images of 11/3/2014, using retrieved OCI/OCx [*Chla*].

We next examine NASA OCI/OCx retrievals of [*Chla*] for these three consecutive granules, Fig. 7a, b and c show the retrieved NASA OCI/OCx [*Chla*] products from these consecutive VIIRS–MODIS–VIIRS images for the WFS near Sarasota FL on 11/3/2014. Data obtained from the National Data Buoy Center website for the C-MAN stations at Venice, FL (Station VENF1). (27°4'21" N 82°27'10" W) gives area wind direction information. Approximate wind and assumed current information is shown overlaid in the retrieval images: Fig. 7.

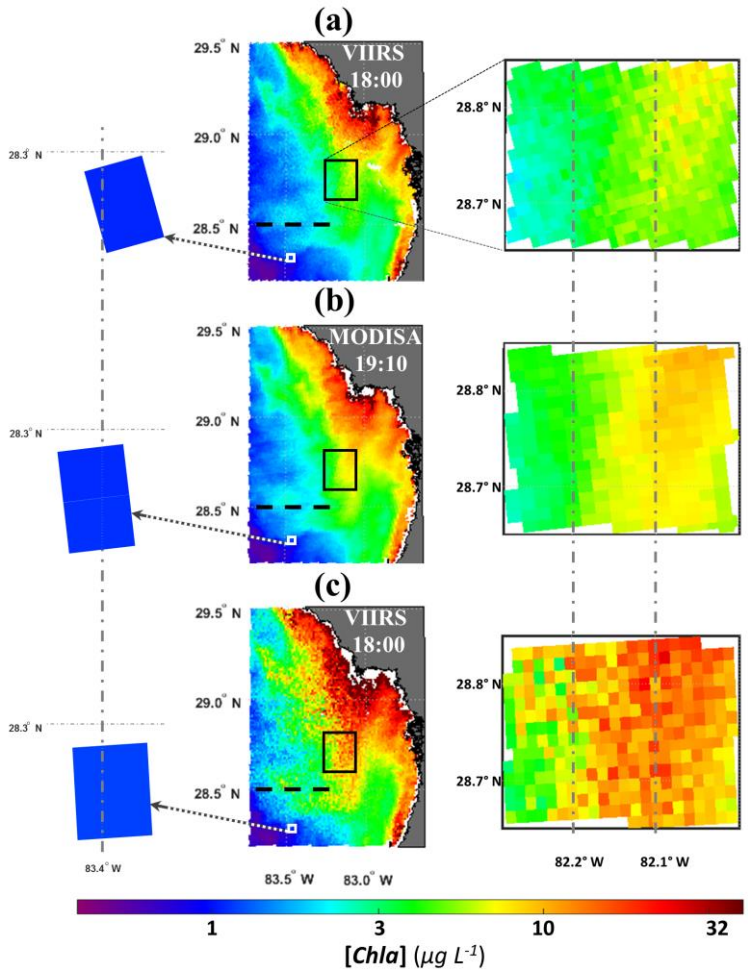


Figure 8 Showing temporal changes in bloom for consecutive satellite images of region 1, 11/3/2014, using retrieved OCI/OCx [*Chla*].

We now examine in more detail Region 1, in Fig. 7, and shown in the zoomed images in Fig. 8. The bloom, as delineated by the [*Chla*] color contour in the zoomed images, appears, qualitatively, to increase in concentration and expand in the southwest direction over the 96-minute interval between the consecutive VIIRS–MODIS–VIIRS overlaps. These changes are reflected in the associated zoomed pixel images (Fig. 8) and appear to provide qualitative visual indications of expansion of the bloom and its increasing [*Chla*] concentration in the southwest direction. This appears broadly consistent with the directions of wind and likely current, though there is no specific or quantitative evidence of linkage. Furthermore, no movements of [*Chla*] distribution patterns are discerned that would indicate transport. Nor is there evidence for identifying specific causes for the changes observed, e.g. whether these are due to upwelling/downwelling effects or otherwise. Note bloom free waters (zoomed blue regions are consistently the same in all 3 images).

For comparison with the VIIRS OCI/OCx retrievals, Figs 7 and 8, which were discussed above, we show in Fig. 9, retrievals using our NN technique for the same consecutive VIIRS overpasses. They show bloom areas and very similar

zoomed-in features as well as bloom free water retrievals (blue). As can be seen, results are qualitatively very similar to those from OCI/OCx, showing bloom expansion to the southwest. Retrieved [*Chla*] values will differ in details, because of the higher accuracies demonstrated by NN (see 3.3 above).

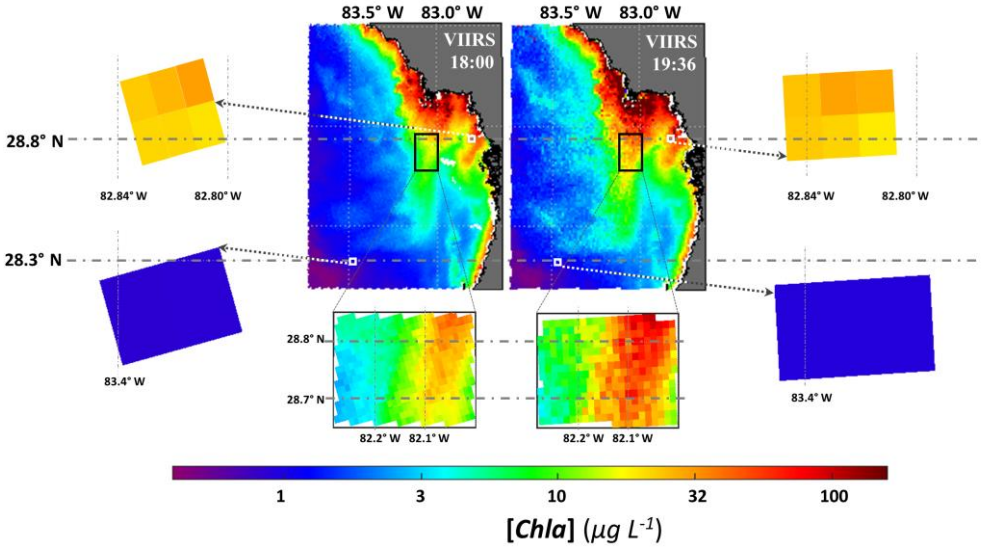


Figure 9 NN VIIRS retrievals of Region 1, 11/3/2014.

Finally, Fig. 10 shows VIIRS and MODIS-A sequential retrievals from Tampa Bay, where a bloom seems first to shrink in [*Chla*] densities opposite to the wind and current direction, then increase again, implying that there are a complexity of factors at work, possibly including down-welling and up-welling.

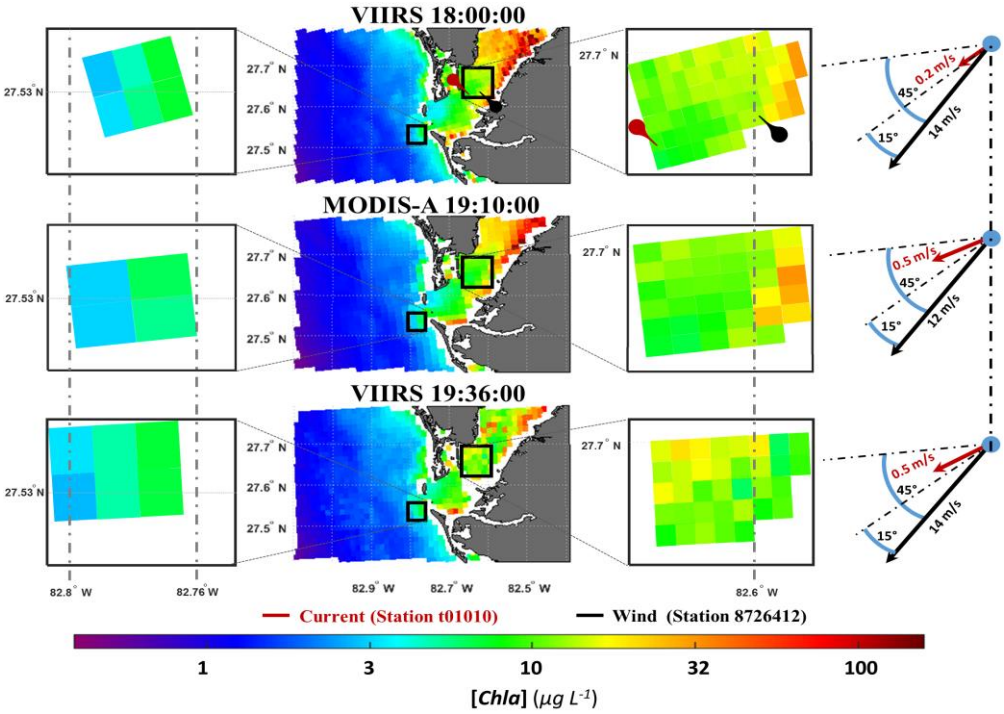


Figure 10 NN retrievals from Tampa Bay, Region 2.

In conclusion, for this section on consecutive satellite images, it is recognized that additional studies that include comparisons from consecutive VIIRS retrievals of *Rrs* values, as well as comparisons of [*Chla*] retrievals against simultaneous in-situ measurements, would be needed to clarify the nature and magnitude of the changes being observed. However, given the difficulty of carrying out comprehensive calibration measurements of this type, we believe that it is reasonable to conclude that while consecutive overlapping satellite images can provide some evidence of temporal changes in *KB* HABs concentration in the WFS, they are unlikely to provide accurate or reliably useful information on the magnitudes involved.

It should also be noted, that while consecutive overlapping images appear to show temporal changes, there is insufficient evidence from them to attribute the relative contributions of drift, patchiness, upwelling/down welling or a combination of any of these to the causes of the changes. The next section, 3.6 presents the results of recent field measurements of *KB* HABs in the WFS, which much more solidly confirm *KB* HABs temporal variabilities as well as patchiness. They also support conclusions that the significantly improved retrieval accuracies that are obtained with shorter overlap time windows between satellite retrievals and in-situ measurements (section 3.3 above) reflect the impact of temporal variabilities.

### 3.5 Field Measurements

The evidence for temporal changes, intra-pixel variations and patchiness associated with blooms in the WFS is further supported more definitively by field measurements made in conjunction with Mote Marine Laboratories on 1/19/2017 off Lido Key, near Sarasota FL. Fig. 11 shows the transect of measurements made. Many of these measurements were made at stations subpixel distances apart (generally 300 meters) on an outward leg, and were then repeated for the same stations as closely as possible on a return leg. Samples were taken at a 0.5 meter depth and cell concentrations obtained by analysis at Mote Marine Laboratories.

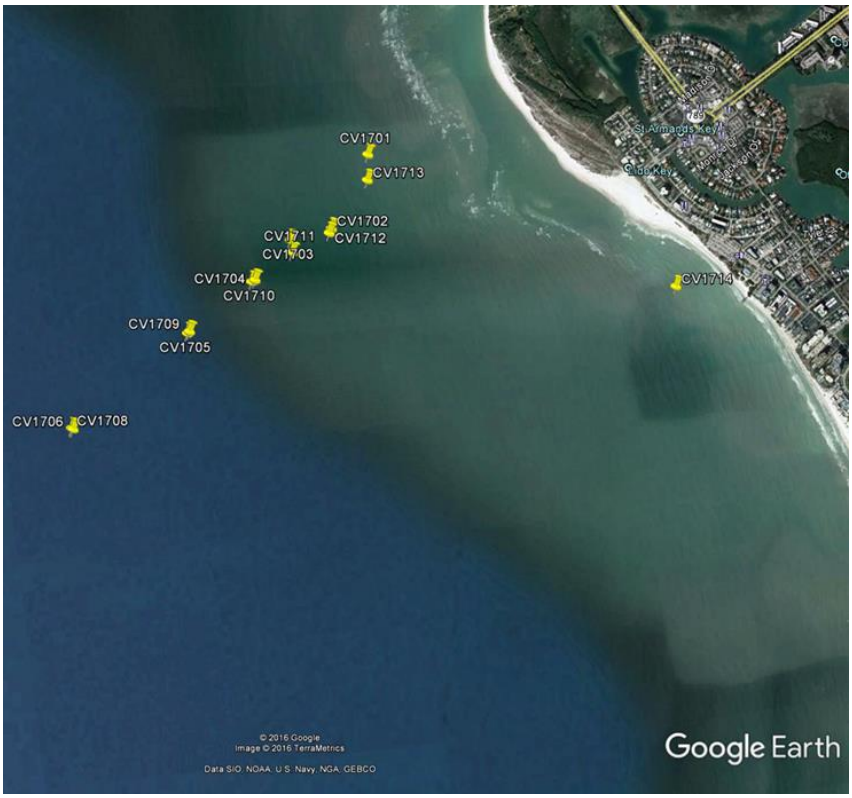


Figure 11 Transect of outward and return legs of field measurements 1/19/2017

Table 5 shows the *KB* cell counts at the different stations and the times of measurement. These are color coded, so that the same row color indicates the results for the same station on both the outward and return leg. It should be noted, that, as might be expected with these high cell counts, the latter showed an excellent match with simultaneous co-located HPLC [*Chla*] measurements. From Table 4 it can be seen that the changes in values at the same station generally increase with the time interval (between outward and return legs). Thus, the greatest change is for Station CV1701 / CV1713 from 7.52 x $10^6$ cells $L^{-1}$ to 1.552 x $10^6$ cells $L^{-1}$ over the 120-minute time interval between the two measurements. The second greatest change is that for the next station, CV1702 / CV1712, where the change is from 1.776 x $10^6$ cells $L^{-1}$ to 1.326 x $10^6$ cells $L^{-1}$ for the 87-minute time interval. For the shortest time between measurements, CV1706 / CV1708 the change is 0.952 x $10^6$ cells $L^{-1}$ to 0.690 x $10^6$ cells $L^{-1}$ over the 21-minute interval between measurements. (It should also be noted that there is also a slight discrepancy in station positions recorded due to drift from measurement start (with GPS initial co-location) to completion and recording.

Table 5. Results of field measurements on 1/19/2017.

| *Station* | *Depth ($m^{-1}$)* | *Lat. (°)* | *Long. (°)* | *Start Time (GMT)* | *End Time (GMT)* | *K. brevis (cells $L^{-1}$)* | *Time diff (minutes)* |
|---|---|---|---|---|---|---|---|
| *CV1701* | 0.7 | 27.31836 | -82.59587 | 17:20 | 17:25 | 7,280,000 | 120 |
| *CV1713* | 0.7 | 27.31713 | -82.59606 | 19:21 | 19:25 | 1,552,000 | |
| *CV1702* | 0.7 | 27.31500 | -82.59831 | 17:48 | 17:52 | 1,776,000 | 87 |
| *CV1712* | 0.7 | 27.31480 | -82.59846 | 19:15 | 19:19 | 1,326,000 | |
| *CV1703* | 0.7 | 27.31467 | -82.60061 | 18:00 | 18:04 | 1,024,000 | 68 |
| *CV1711* | 0.7 | 27.31408 | -82.60059 | 19:09 | 19:12 | 1,110,000 | |
| *CV1704* | 0.7 | 27.31296 | -82.60277 | 18:07 | 18:12 | 964,000 | 54 |
| *CV1710* | 0.7 | 27.31289 | -82.60298 | 19:03 | 19:06 | 590,000 | |
| *CV1705* | 0.7 | 27.31077 | -82.60677 | 18:18 | 18:22 | 642,000 | 37 |
| *CV1709* | 0.7 | 27.31085 | -82.60664 | 18:55 | 18:59 | 576,000 | |
| *CV1706* | 0.7 | 27.30681 | -82.61356 | 18:27 | 18:32 | 952,000 | 21 |
| *CV1708* | 0.7 | 27.30686 | -82.61364 | 18:48 | 18:51 | 690,000 | |

These results illustrate both the intra pixel variations that can typically occur (as well as inter pixel variations) and confirm the temporal variations that can be expected. The relative contributions of drift or upwelling/downwelling to the results are not examined here. In general, the consecutive satellite images and the field measurements observations lend support to our underlying thesis that the significantly increased bloom retrieval accuracy that occurs by shortening of the overlap time window between observation and in-situ measurement match-ups from 100 minutes to 15 minutes, is due to temporal changes in the observed bloom. They also serve to underline that magnitudes derived from satellite observations may only be valid for brief periods. To deal with these uncertainties, we are currently examining temporal and spatial averaging possibilities. It should be noted that sampling depths can also result in considerable variability in measured values. For instance, a typical set of measurements of *KB* HABs in the WFS in a 2018 cruise, were for 0.1, 0.5 and 1 meter sampling depths, cell counts/liter were 4424000, 5037000 and 2351000.

### 3.8 Different algorithm retrievals, using in-situ radiometric measurements and their available satellite match-ups as inputs, are compared against in-situ sample measurements.

Better performance of NN VIIRS retrievals against in-situ measurements may be due to relative invulnerability of longer wavelengths used (481, 551, 671 nm) to atmospheric correction inadequacies impacting shorter wavelengths used in other algorithms, particularly for closer in-shore waters. To eliminate atmospheric correction inadequacy concerns, comparisons were made of different algorithm retrievals using in-situ radiometric measurements against in-situ sample measurements – for a variety of waters – both in-shore and off-shore. We extended the retrievals test of NN, OCI/OCx , QAA and RGCI algorithms for different water types: Open Ocean, Coastal and *KB* bloom waters. The 43 non-bloom in-situ and satellite Open Ocean measurements are from the NOAA VIIRS Calibration and Validation cruises [37-39] over the 2014-16 period. The 40 coastal *KB* HABs bloom in-situ measurements are from our 2017 and 2018 WFS field

campaigns. Both datasets are included in the comparisons. Fig.12 shows the location of all bloom and non-bloom in-situ measurements.

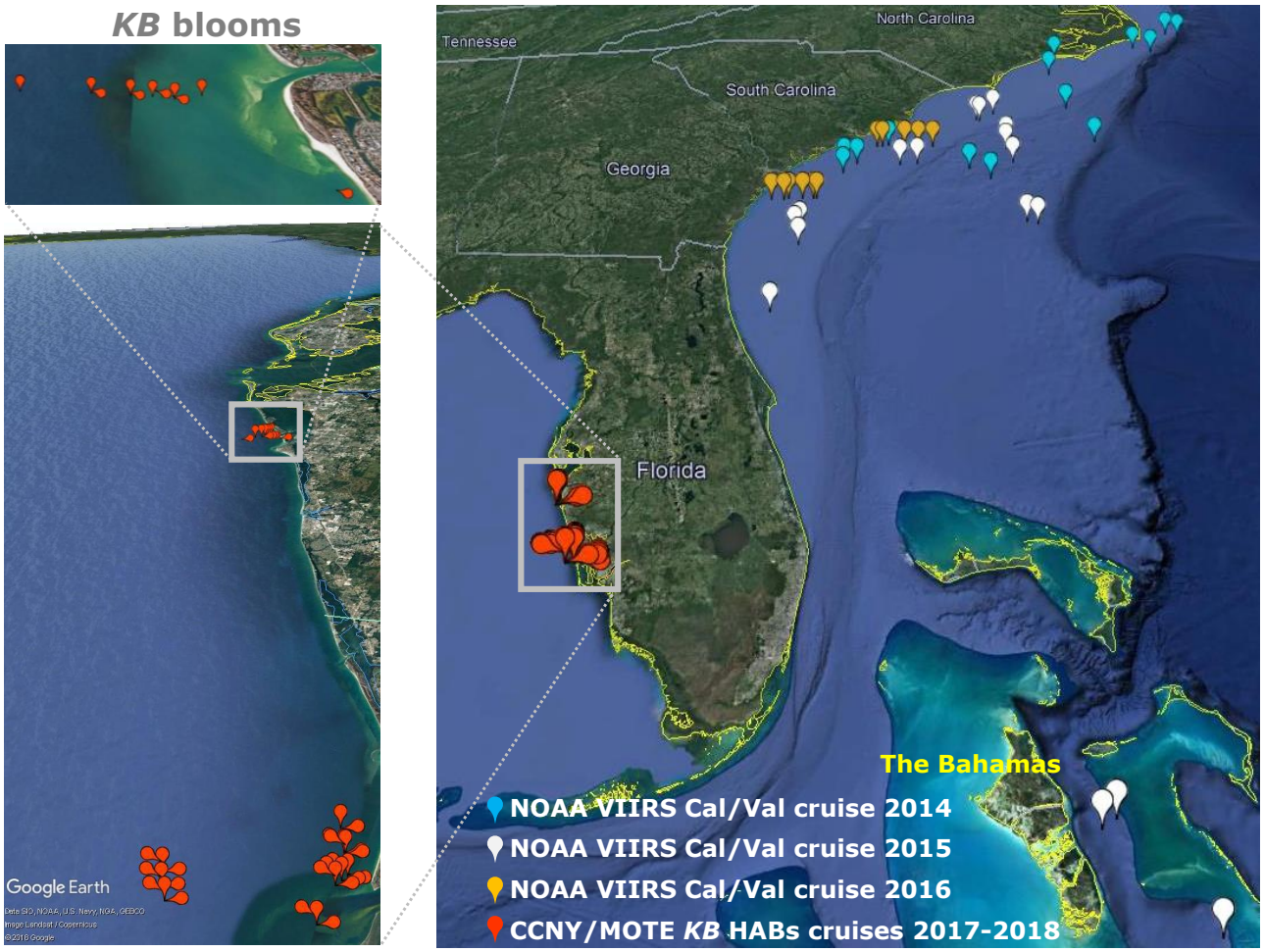


Fig.12 Locations for in-situ radiometric and sample measurements used in retrieval comparisons, Sites in the WFS were *KB* HABs sites where 40 *KB* HABs cell count measurements sample were obtained (and converted to [*Chla*]) and in-situ radiometric measurements made. In Atlantic coast sites, 43 sample measurements were taken and [*Chla*] measured, and both in-situ and VIIRS satellite radiometric data obtained.

Retrieval regression statistics are shown in Fig 13. The top row shows retrievals obtained for different algorithms using in-situ radiometric retrievals as inputs, and sample measurements for all 83 stations. This includes 40 complex coastal water measurements in the WFS with *KB* HABs from our 2017 and 2018 field campaigns, as well as 43 Open Ocean measurements on Atlantic coasts. The bottom row shows the available satellite match-ups retrievals compared against the in-situ sample measurements for these same 83 measurements. As can be seen in Fig. 13, retrieval accuracies are improved (top row) for all algorithms that use in-situ radiometric measurements as inputs, than the 47 qualitatively similar retrievals from satellites, for all the algorithms considered. The statistics of these retrievals are summarized in Table 6 below.

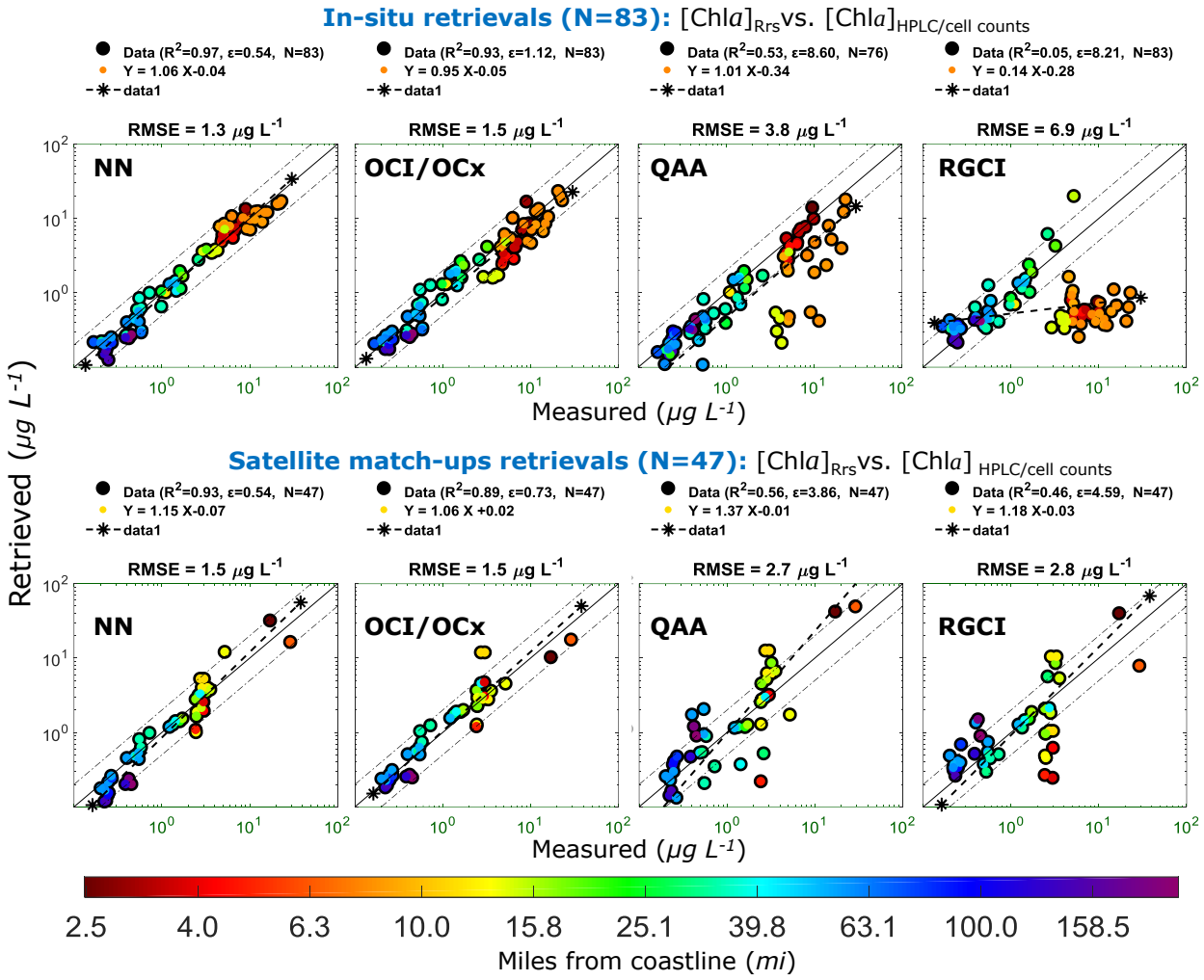


**Figure 13.** Results for NN, OCI/OCx, RGCI, and QAA retrievals in the WFS and Atlantic coasts. The top row shows retrievals obtained for different algorithms using in-situ radiometric retrievals and sample measurements for all 83 stations. This includes 40 measurements in the WFS with *KB* HABs, as well as 43 Open Ocean measurements on Atlantic coasts. The bottom row shows satellite retrievals compared against the in-situ sample measurements for the match-ups available of Open Ocean, coastal and *KB* HABs waters in the WFS regions. Color coding of the dots denotes distance to shore, with red being the closest. Statistics for these retrievals are summarized in table 6 below.

**Table 6** Statistics of comparison for Fig. 13:

| *y-axis* [Chla] ($\mu g \cdot L^{-1}$) | *x-axis* [Chla] ($\mu g \cdot L^{-1}$) | $R^2$ | RMSE | Slope & Intercept | N |
|---|---|---|---|---|---|
| *NN* | **In-situ ($R_{rs}$) retrievals** | 0.97 | 1.3 | $y = 1.06x - 0.04$ | 83 |
| *OCI/OCx* | | 0.93 | 1.5 | $y = 0.95x - 0.05$ | 83 |
| *QAA* | | 0.53 | 3.8 | $y = 1.01x - 0.34$ | 83 |
| *RGCI* | | 0.05 | 6.9 | $y = 0.14x - 0.28$ | 83 |
| *NN* | **Satellite ($R_{rs}$) match-ups retrievals** | 0.93 | 1.5 | $y = 1.15x - 0.07$ | 47 |
| *OCI/OCx* | | 0.89 | 1.5 | $y = 1.06x + 0.02$ | 47 |
| *QAA* | | 0.56 | 2.7 | $y = 1.37x - 0.01$ | 47 |
| *RGCI* | | 0.46 | 2.8 | $y = 1.18x - 0.03$ | 47 |

Retrieval performance for the different algorithms is also examined by comparing the residuals (difference between retrieved values and sample measurements) at varying distances from the shoreline. These are shown in Fig. 14 below for both open ocean (Atlantic) and complex coastal *KB* HABs water in WFS. In both cases in-situ radiometric Rrs values and measured samples were used.

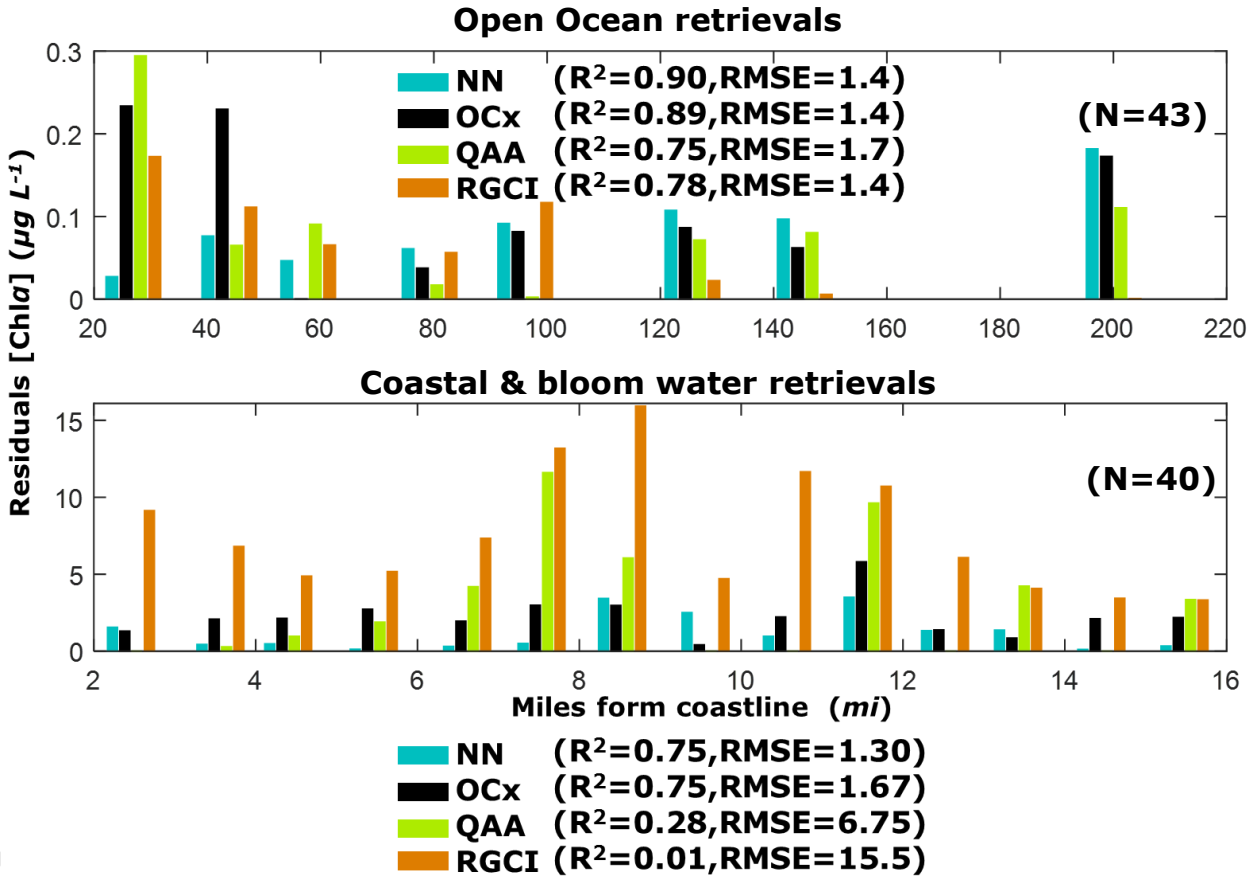


Fig. 14. Residuals (difference between retrieved values and sample measurements) at varying distances from the shoreline for the different algorithms.

As can be seen from Fig. 13 and 14 above, for the coastal water regions located 2 to 16 miles from shoreline, the NN algorithm exhibited the lowest retrieval errors and RMSE of ~ 1.3. For the Open Ocean regions all algorithms exhibited similar errors with RMSE ~ 1.4. The regression lines in Fig. 13 seems to improve in OCI/OCx for the low chlorophyll-a retrieved values and in NN for the high chlorophyll-a retrieved values. In general, for the more complex WFS waters with *KB* HABs, the NN algorithm performs better, closely followed by OCI/OCx. This would tend to support the notion that higher accuracies of NN retrievals may be at least partially due to the use of longer Rrs input wavelengths for NN, than the deeper blue wavelengths used with other algorithms. Thereby lessening the impact that inadequate atmospheric corrections associated with deeper blue wavelengths will affect retrieval accuracies, as well as possible reduced spectral interference by the existence CDOM (expected in more complex waters).

These possibilities are lent additional credence by examining retrieval using the NASA OCI/OCx algorithm applied to the previous sets of 40 WFS and 43 Open Ocean Atlantic coast measurements. Results of these retrievals are shown in Fig. 15 below. The left hand side shows retrievals for all 83 measurements (40 *KB* HABs complex waters and 43 Atlantic Open Ocean waters) using in-situ radiometric measurements as inputs compared against sample measurements. The top left hand corner image shows retrievals using the NASA OCI/OCx algorithm with 443 nm as

input. The bottom left hand corner image shows these same retrievals using the NASA OCI/OCx algorithm, but now with 486 nm as input instead of 443 nm.

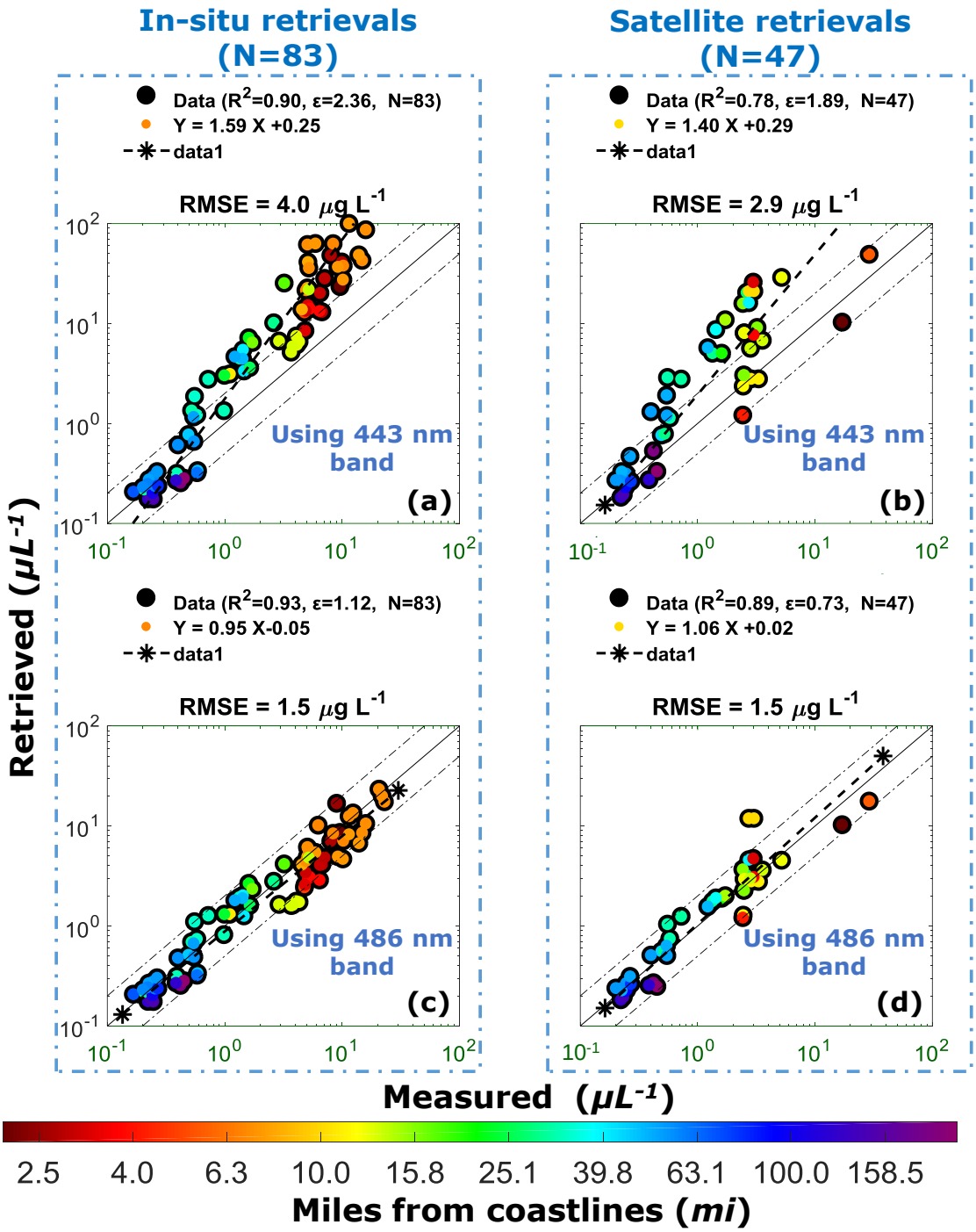


**Figure 15** Shows OCI/OCx retrieval regression when using VIIRS 443 band (top row) and VIIRS 486 band (bottom row). **(a & c)** shows in-situ $R_{rs}$ [*Chla*] retrievals **(b & d)** shows satellite $R_{rs}$ [*Chla*] retrievals. OCI/OCx retrieval statistics show improvements when using VIIRS 486 nm instead of 443.

As can be seen, better accuracies are obtained with the 486 nm input. On the top right hand side, Fig. 15 shows VIIRS NASA OCI/OCx satellite retrievals for the 43 open ocean measurements using 443 nm as input. The bottom right hand corner shows VIIRS OCI/OCx retrievals for the same 43 open ocean points, but using 486 nm as input instead of 443 nm. As can be seen, the OCI/OCx retrievals with inputs with 486 nm instead of 443 nm give the higher retrieval accuracies, as did the retrievals obtained with the in-situ radiometric measurements as inputs. Again, this tends to confirm that the longer wavelengths used as inputs to the retrieval algorithms are advantageous, whether due to lesser vulnerability to inadequate atmospheric correction, and/or to lesser spectral interference from CDOM, particularly in complex waters.

## 4. SUMMARY AND CONCLUSIONS

In the work reported here, NN algorithms using *Rrs* values from the 486, 551 and 671 nm VIIRS bands are used to retrieve an image of $a_{ph443}$ values in the WFS. Then, additional limiting constraints are applied, in two filter processes, requiring $a_{ph443}$ to be above a limiting value, and backscatter and hence Rrs 551 to be below a limiting value, thus eliminating from the retrieved $a_{ph443}$ image all pixels which are not compatible with the existence of *KB* HABs. The residual image then shows only retrieved $a_{ph443}$ values and their equivalent [*Chla*] values that are consistent with the existence of *KB* HABs.

Retrievals of *KB* HABs in the WFS from VIIRS overpasses, using NN were then compared with other retrievals using other algorithms including OCI/OCx, GIOP, QAA and RGCI against in-situ sample measurements. For meaningful quantitative comparisons, it is important to have many data points. Accordingly, we sought all available match-ups between VIIRS NN $a_{ph443}$ (and equivalent [*Chla*] retrievals) and *in situ KB* cell count measurements for the period 2012–2016, as well as from our own measurements with Mote marine in 2017-2018. These comparisons showed that for VIIRS observations, the NN technique appeared to offer good potential for effective retrievals of *KB* HABs cell counts in the WFS, and analysis of retrieval statistics showed the NN technique to be the most accurate, followed by NASA's OCI/OCx. However, more comparisons also showed that when the window between *in situ* observations and satellite overpass measurements was reduced from 100 minutes to 15 minutes, retrieval accuracies greatly improved, with increased correlations and reduced errors. This is now understood to be due to the temporal change in the *KB* HABs scene being observed. That these temporal changes can occur fairly rapidly, was confirmed unambitiously by retrievals of *KB* HABs images in the WFS from consecutive VIIRS –MODIS-VIIRS overpasses, as well as field campaigns making in-situ *KB* HABs measurements in the WFS.

The higher retrieval accuracies of *KB* HABs obtained with NN in the WFS, may be explained by the fact that the NN retrieval algorithm uses longer wavelengths than the deep blue wavelengths used by other retrieval algorithms. The longer wavelengths used are less vulnerable to atmospheric correction inadequacies, as well as to spectral interference from CDOM, both of which are factors likely to be present in the complex *KB* HABs coastal waters of the WFS. It is also important to note that the higher accuracies of NN retrievals may also be inherent because of the training used in the evolution of the NN algorithm. This was based on a very wide and comprehensive variety of global observations, representing ranges and distributions that are typical for both coastal and oceanic water conditions.To shed more light on these questions, retrieval comparisons were carried out in the complex waters of the WFS and in open ocean waters on the Atlantic coasts. In-situ radiometric measurement were carried out along with the sampling procedures. Comparisons of NN retrievals with other algorithms were then carried out using the in-situ radiometric measurements as inputs to the algorithms. All retrievals, both those from satellite observations and those from in-situ radiometric measurements and were then compared with the sample measurements. Analysis of retrieval statistics again showed NN have the best performance in complex coastal waters, followed by OCI/OCx in complex waters.

Finally, the case for the advantages of longer wavelengths inputs in the retrieval algorithms was reinforced by examination of retrievals using the OCI/OCx algorithms with input at 443 or 486 nm, which are available as NASA products. These comparisons were carried out with one set using the in-situ radiometric measurements as inputs, while the other examined satellite retrievals. Again, both sets of retrievals were compared against the in-situ sample measurements. For each set the OCI/OCx algorithm using 486 nm as inputs performed better than the one using 443 nm.

In general, it can be concluded that NN retrievals are effective for retrieving *KB* HABs in complex coastal waters such as the WFS. Analysis of retrieval statistics against sample measurements show NN performs better in complex coastal waters than other algorithms The use of longer Rrs input wavelengths may make NN them less vulnerable to atmospheric correction inadequacies and CDOM spectral interference than algorithms, which use deep blue input wavelengths which generally impact retrievals in complex coastal waters. It is important to note that temporal variabilities associated with *KB* HABs impact and limit the utility of satellite retrievals, and suggest the use of other observation platforms, possibly including UAVs.

## Abbreviations

The following abbreviations are used in this manuscript:

| | |
|---|---|
| *KB* | *Karenia brevis* |
| HABs | Harmful algal blooms |
| WFS | West Florida Shelf |
| VIIRS | Visible Infrared Imaging Radiometer Suite |
| MODIS-A | Moderate Resolution Imaging Spectroradiometer Aqua |
| MERIS | MEdium Resolution Imaging Spectrometer |
| $a_{ph}$ | Absorption coefficient due to phytoplankton particulates ($m^{-1}$) |
| $a_{dg}$ | Absorption coefficient due to non-phytoplankton particulates and dissolved substances, $a_{dm} + a_g$ ($m^{-1}$) |
| $a_{dm}$ | Absorption coefficient due to non-phytoplankton particulates ($m^{-1}$) |
| $a_w$: | Absorption coefficient due to water ($m^{-1}$) |
| $a_t$ | Total absorption coefficient, $a_{ph} + a_{dm} + a_g + a_w$ ($m^{-1}$) |
| $b_{bp}$ | Backscattering coefficient due to particulates ($m^{-1}$) |
| $b_{bw}$ | Backscattering coefficient due to water ($m^{-1}$) |
| $b_b$ | Total backscattering coefficient, $b_{bp} + b_{bw}$ ($m^{-1}$) |
| [*Chla*] | Chlorophyll-*a* concentration ($\mu g \cdot L^{-1}$) |
| CDOM | Color dissolved organic matter (ppm) |
| NAP | Non-phytoplankton particulate concentration ($g \cdot m^{-3}$) |
| AOP | Apparent optical properties |
| IOP | Inherent Optical properties |
| RT | Radiative transfer |
| *Rrs* | Above-surface remote-sensing reflectance ($sr^{-1}$) |
| *nLw* | Normalized water leaving radiance ($W \cdot m^{-2} \cdot \mu m \cdot sr^{-1}$) |
| MLPNN | Multi Layer perceptron neural network |
| NN | Neural network |
| NN [*Chla*] | NN deriving [*Chla*] from *Rrs* as inputs |
| NOMAD | NASA bio-Optical Marine Algorithm Data set [22]. |
| nFLH | Normalized fluorescence height Algorithm ($W \cdot m^{-2} \cdot \mu m \cdot sr^{-1}$) [55]. |
| RBD | Red Band Difference Algorithm ($W \cdot m^{-2} \cdot \mu m \cdot sr^{-1}$). [5,6] |
| OC | Ocean Color |
| OC3 | Chlorophyll-*a* concentration ($\mu g \cdot L^{-1}$) derived using VIIRS and MODIS algorithm [40–42]. |
| OCI | Chlorophyll-*a* concentration ($\mu g \cdot L^{-1}$) derived using VIIRS and MODIS algorithm [40]. |
| RGCI | Red Green chlorophyll-*a* Index |
| GIOP | Generalized Inherent Optical Property |
| QAA | Quasi-Analytical Algorithm version |
| $R^2$ | Coefficient of determination. Orthogonal linear regression approach was used. |
| $\varepsilon$ | Error – sum of orthogonal distances. |
| N | Number of points |
| $\mu$ | Mean value |
| HPLC | High Performance Liquid Chromatography |
| MOTE | Mote Marine Laboratory |


## Acknowledgments

This work was partially supported by grants from NOAA through NOAA CREST, and NOAA JPSS.

## REFERENCES


[1] A. El-Habashi, I. Ioannou, M. Tomlinson *et al.*, "Satellite Retrievals of Karenia brevis Harmful Algal Blooms in the West Florida Shelf Using Neural Networks and Comparisons with Other Techniques," Remote Sensing, 8(5), 377 (2016).

[2] A. El-Habashi, C. M. Duran, V. Lovko *et al.*, "Satellite retrievals of Karenia brevis harmful algal blooms in the West Florida shelf using neural networks and impacts of temporal variabilities," Journal of Applied Remote Sensing, 11(3), 032408-032408 (2017).

[3] C. Hu, F. E. Muller-Karger, C. J. Taylor *et al.*, "Red tide detection and tracing using MODIS fluorescence data: A regional example in SW Florida coastal waters," Remote Sensing of Environment, 97(3), 311-321 (2005).

[4] R. Amin, J. Zhou, A. Gilerson *et al.*, "Novel optical techniques for detecting and classifying toxic dinoflagellate Karenia brevis blooms using satellite imagery," Optics express, 17(11), 9126-9144 (2009).

[5] M. Tomlinson, T. Wynne, and R. Stumpf, "An evaluation of remote sensing techniques for enhanced detection of the toxic dinoflagellate, Karenia brevis," Remote Sensing of Environment, 113(3), 598-609 (2009).

[6] G. A. Carvalho, P. J. Minnett, V. F. Banzon *et al.*, "Long-term evaluation of three satellite ocean color algorithms for identifying harmful algal blooms (Karenia brevis) along the west coast of Florida: A matchup assessment," Remote sensing of environment, 115(1), 1-18 (2011).

[7] D. Blondeau-Patissier, J. F. Gower, A. G. Dekker *et al.*, "A review of ocean color remote sensing methods and statistical techniques for the detection, mapping and analysis of phytoplankton blooms in coastal and open oceans," Progress in oceanography, 123, 123-144 (2014).

[8] C. Hu, B. B. Barnes, L. Qi *et al.*, "A harmful algal bloom of Karenia brevis in the Northeastern Gulf of Mexico as revealed by MODIS and VIIRS: A comparison," Sensors, 15(2), 2873-2887 (2015).

[9] I. M. Soto, J. Cannizzaro, F. E. Muller-Karger *et al.*, "Evaluation and optimization of remote sensing techniques for detection of Karenia brevis blooms on the West Florida Shelf," Remote Sensing of Environment, 170, 239-254 (2015).

[10] I. Ioannou, A. Gilerson, B. Gross *et al.*, "Neural network approach to retrieve the inherent optical properties of the ocean from observations of MODIS," Applied Optics, 50(19), 3168-3186 (2011).

[11] I. Ioannou, A. Gilerson, B. Gross *et al.*, "Deriving ocean color products using neural networks," Remote Sensing of Environment, 134, 78-91 (2013).

[12] I. Ioannou, A. Gilerson, M. Ondrusek *et al.*, "Remote estimation of in water constituents in coastal waters using neural networks." In Proc. of SPIE Vol, vol. 9240, pp. 92400T-1. 2014.

[13] A. El-habashi, and S. Ahmed, "Neural network algorithms for retrieval of harmful algal blooms in the west Florida shelf from VIIRS satellite observations and comparisons with other techniques, without the need for a fluorescence channel." 96380B-96380B-12.

[14] C. Le, and C. Hu, "A hybrid approach to estimate chromophoric dissolved organic matter in turbid estuaries from satellite measurements: A case study for Tampa Bay," Optics express, 21(16), 18849-18871 (2013).

[15] J. P. Cannizzaro, C. Hu, D. C. English *et al.*, "Detection of Karenia brevis blooms on the west Florida shelf using in situ backscattering and fluorescence data," Harmful Algae, 8(6), 898-909 (2009).

[16] P. J. Werdell, and S. W. Bailey, "An improved in-situ bio-optical data set for ocean color algorithm development and satellite data product validation," Remote sensing of environment, 98(1), 122-140 (2005).

[17] C. D. Mobley, [Light and water: radiative transfer in natural waters] Academic press, (1994).

[18] R. M. Pope, and E. S. Fry, "Absorption spectrum (380–700 nm) of pure water. II. Integrating cavity measurements," Applied optics, 36(33), 8710-8723 (1997).

[19] A. M. Ciotti, M. R. Lewis, and J. J. Cullen, "Assessment of the relationships between dominant cell size in natural phytoplankton communities and the spectral shape of the absorption coefficient," Limnology and Oceanography, (2002).

[20] Z. Lee, K. L. Carder, and R. A. Arnone, "Deriving inherent optical properties from water color: a multiband quasi-analytical algorithm for optically deep waters," Applied optics, 41(27), 5755-5772 (2002).

[21] Z. Lee, "Reports of the International Ocean-Colour Coordinating Group: Fundamentals, Tests of Algorithms, and Applications, Report 5," (2006).

[22] C. D. Mobley, and L. K. Sundman, "Hydrolight 4.2 technical documentation," Sequoia Scientific, Incorporated, Redmond, WA, 98052, 84 (2001).

[23] F. Aires, C. Prigent, W. Rossow *et al.*, "A new neural network approach including first-guess for retrieval of atmospheric water vapor, cloud liquid water path, surface temperature and emissivities over land from satellite microwave observations," (2000).
[24] NASA's OceanColor Web by the Ocean Biology Processing Group (OBPG) at NASA's Goddard Space Flight Center. Chlorophyll-a algorithm. (Accessed on 22 November 2016), Available online: https://oceancolor.gsfc.nasa.gov/atbd/chlor_a/.
[25] L. Qi, C. Hu, J. Cannizzaro *et al.*, "VIIRS Observations of a Karenia brevis Bloom in the Northeastern Gulf of Mexico in the Absence of a Fluorescence Band," IEEE Geoscience and Remote Sensing Letters, 12(11), 2213-2217 (2015).
[26] J. Werdell, "Global Bio- optical Algorithms for Ocean Color Satellite Applications: Inherent Optical Properties Algorithm Workshop at Ocean Optics XIX; Barga, Italy, 3–4 October 2008," Eos, Transactions American Geophysical Union, 90(1), 4-4 (2009).
[27] P. J. Werdell, B. A. Franz, S. W. Bailey *et al.*, "Generalized ocean color inversion model for retrieving marine inherent optical properties," Applied optics, 52(10), 2019-2037 (2013).
[28] P. J. Werdell, B. A. Franz, J. T. Lefler *et al.*, "Retrieving marine inherent optical properties from satellites using temperature and salinity-dependent backscattering by seawater," Optics express, 21(26), 32611-32622 (2013).
[29] Z. P. Lee, QAA Algorithm (Accessed on 22 November 2016), Available online: http://ioccg.org/groups/Software_OCA/QAA_v5.pdf.
[30] Z. Lee, and K. L. Carder, "Absorption spectrum of phytoplankton pigments derived from hyperspectral remote-sensing reflectance," Remote Sensing of Environment, 89(3), 361-368 (2004).
[31] C. Hu, Z. Lee, and B. Franz, "Chlorophyll aalgorithms for oligotrophic oceans: A novel approach based on three- band reflectance difference," Journal of Geophysical Research: Oceans, 117(C1), (2012).
[32] J. E. O'Reilly, S. Maritorena, B. G. Mitchell *et al.*, "Ocean color chlorophyll algorithms for SeaWiFS," Journal of Geophysical Research: Oceans, 103(C11), 24937-24953 (1998).
[33] P. J. Franks, "Spatial patterns in dense algal blooms," Limnology and Oceanography, 42(5), 1297-1305 (1997).
[34] R. Stumpf, M. Culver, P. Tester *et al.*, "Monitoring Karenia brevis blooms in the Gulf of Mexico using satellite ocean color imagery and other data," Harmful Algae, 2(2), 147-160 (2003).
[35] L. Leng, T. Zhang, L. Kleinman *et al.*, "Ordinary least square regression, orthogonal regression, geometric mean regression and their applications in aerosol science." 78, 012084.
[36] R. Arnone, R. Vandermeulen, S. Ladner *et al.*, "Diurnal changes in ocean color in coastal waters." 982711-982711-8.
[37] M. Ondrusek, and V. P. Lance, "Report for Dedicated JPSS VIIRS Ocean Color Calibration/Validation Cruise," (2015).
[38] M. Ondrusek, V. P. Lance, M. Wang *et al.*, "Report for dedicated JPSS VIIRS Ocean Color December 2015 Calibration/Validation Cruise," (2016).
[39] M. Ondrusek, V. P. Lance, M. Wang *et al.*, [Report for Dedicated JPSS VIIRS Ocean Color Calibration/Validation Cruise October 2016], (2017).